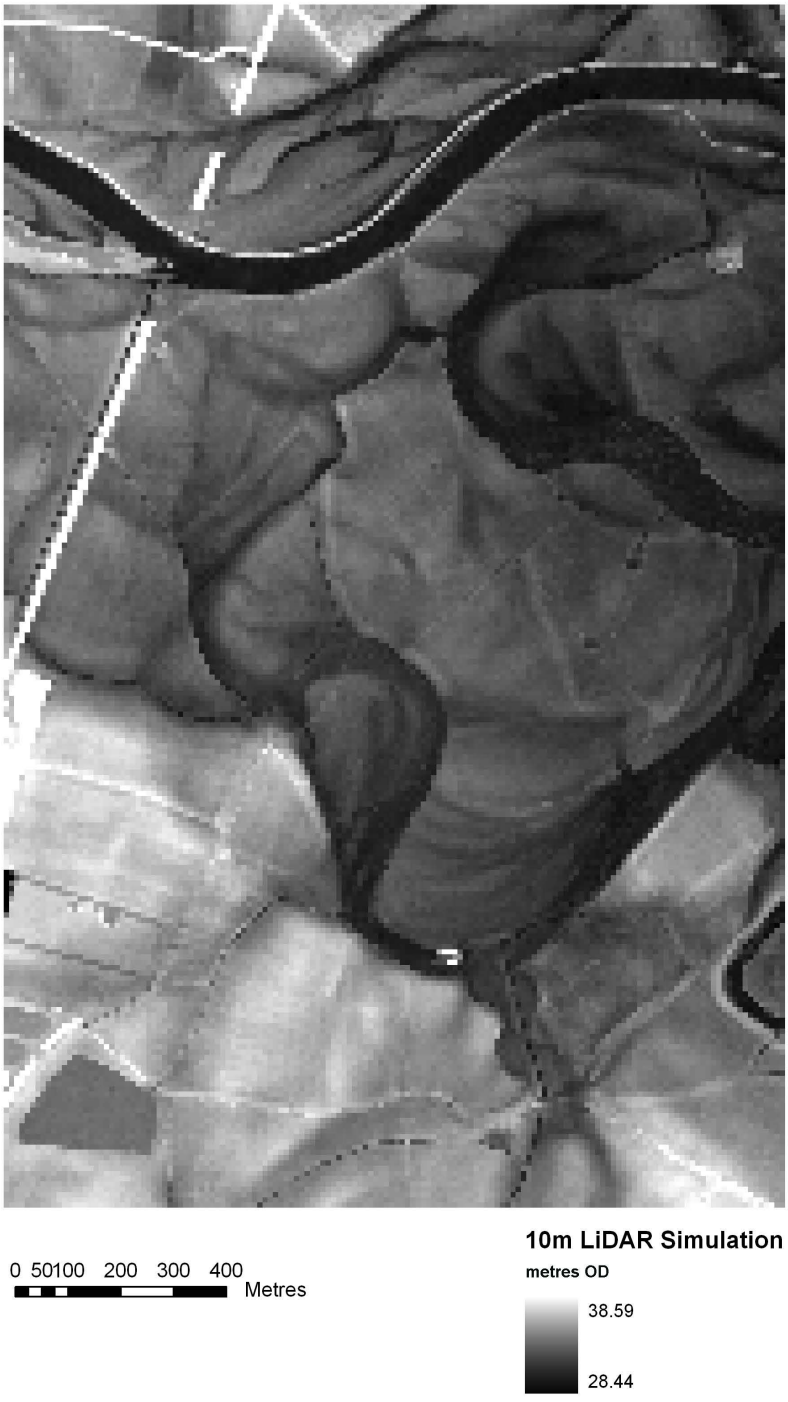

Fig 4.26: Simulated 10m LiDAR Last pulse ground digital surface model.

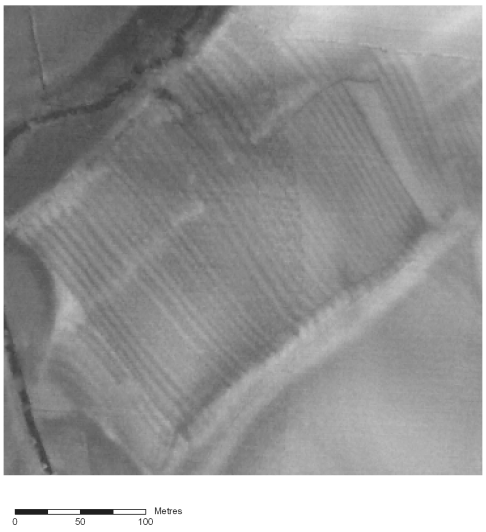

1m

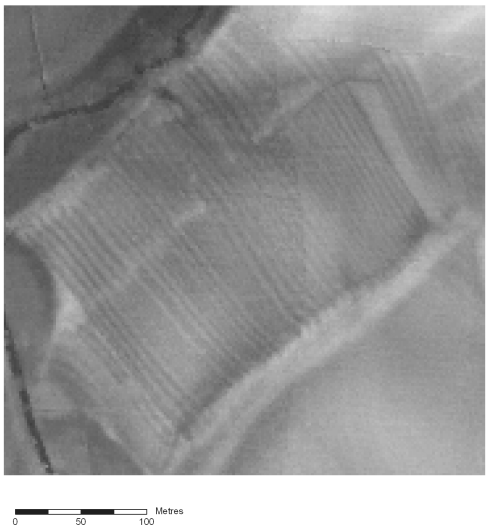

2m

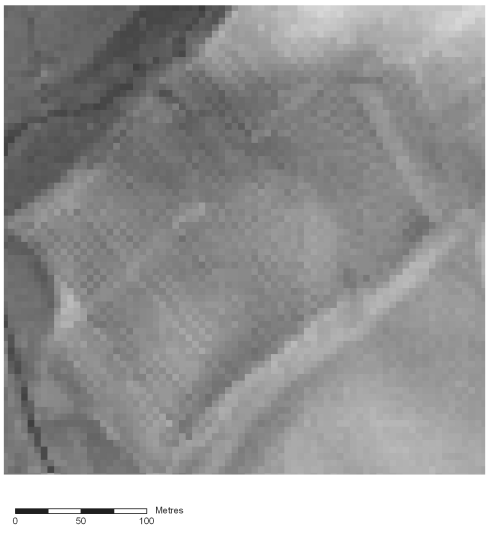

5m

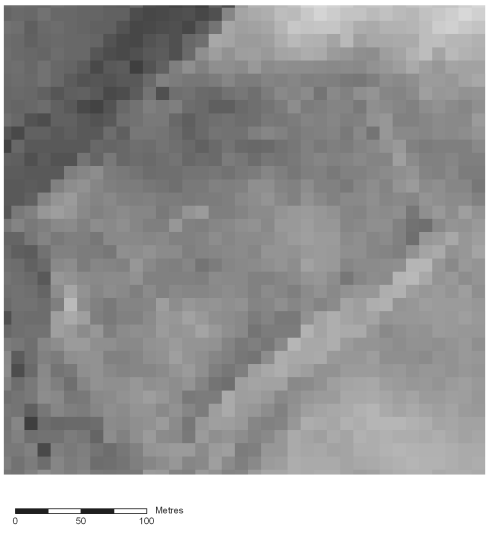

10m

Fig 4.27: LiDAR DSM of an area of earthwork ridge and furrow in the southeast corner of the study area showing the impact of variations in spatial resolution.

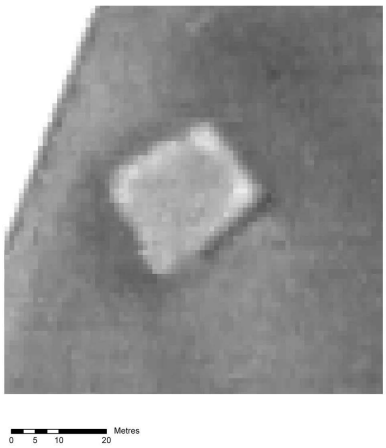

1m

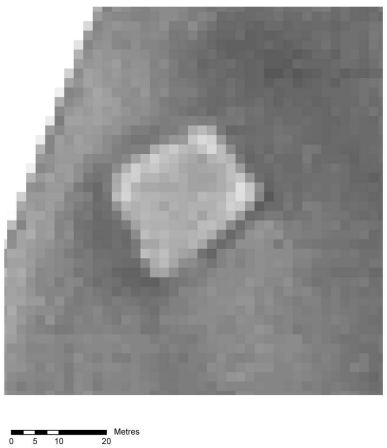

2m

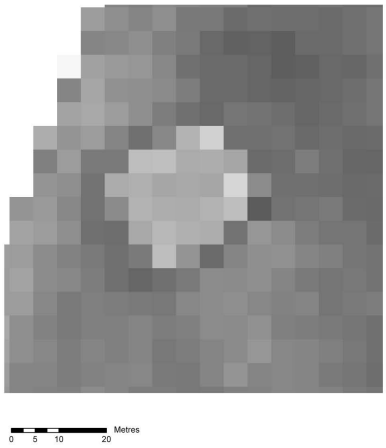

5m

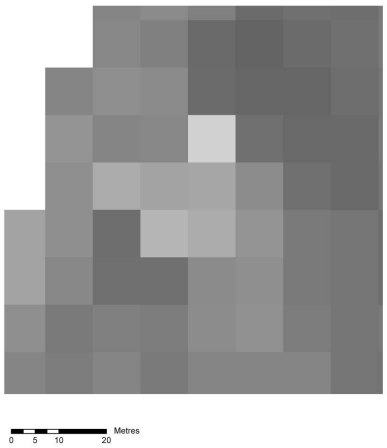

10m

Fig 4.28: LiDAR DSM of the earthworks of the Bull Ring in the northwest corner of the study area showing the impact of variations in spatial resolution.

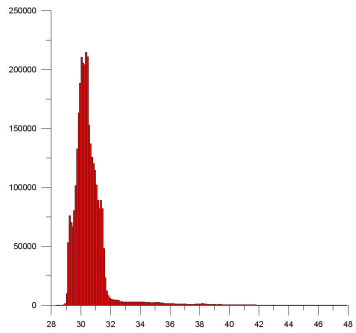

LiDAR 1m First Pulse DSM

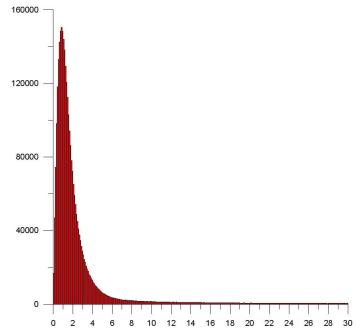

LiDAR 1m First Pulse Slope

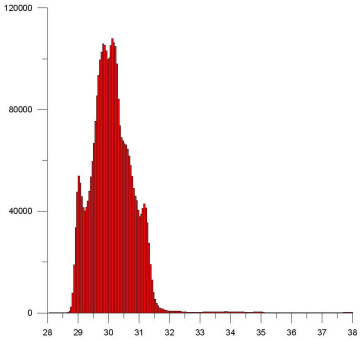

LiDAR 1m Last Pulse DSM

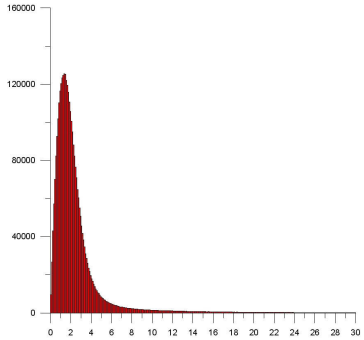

LiDAR 1m Last Pulse Slope

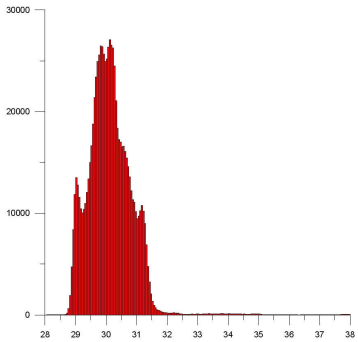

LiDAR 2m Last Pulse DSM

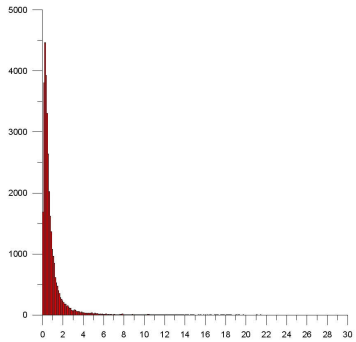

LiDAR 2m Last Pulse Slope

Fig 4.29: Elevation (left) and slope (right) histograms for LiDAR 1mFP, 1mLP and 2m DSM data for the entire study area.

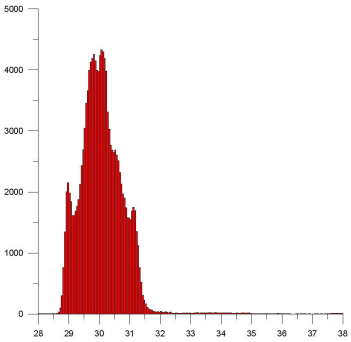

LiDAR 5m Last Pulse DSM

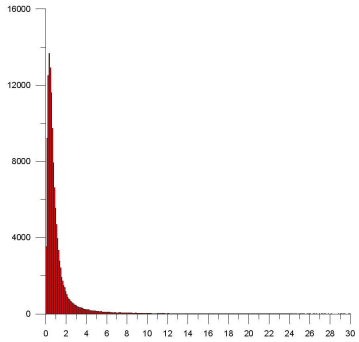

LiDAR 5m Last Pulse Slope

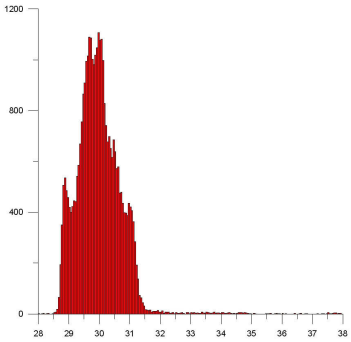

LiDAR 10m Last Pulse DSM

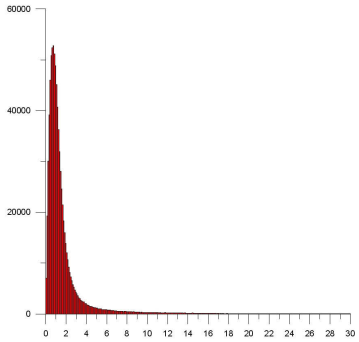

LiDAR 10m Last Pulse Slope

Fig 4.30: Elevation (left) and slope (right) histograms for LiDAR 5m, and 10m DSM data for the entire study area.

DSM 1m FPA			DSM 1m LPG		DSM 2m LPG	
Number of values	3355744	Number of values	Number of values	3355744	Number of values	839504
Minimum	23.69	Minimum	Minimum	28.29	Minimum	28.29
Maximum	56.07	Maximum	Maximum	38.74	Maximum	38.71
Range	32.38	Range	Range	10.45	Range	10.42
Mean	30.621	Mean	Mean	30.388	Mean	30.388
Standard deviation	1.4704	Standard deviation	Standard deviation	0.75695	Standard deviation	0.75738
Skew	4.784	Skew	Skew	2.276	Skew	2.279

DSM 5m LPG		DSM 10m LPG	
Number of values	134680	Number of values	33744
Minimum	28.31	Minimum	28.44
Maximum	38.6	Maximum	38.6
Range	10.29	Range	10.16
Mean	30.39	Mean	30.393
Standard deviation	0.75916	Standard deiation	0.76173
Skew	2.285	Skew	2.292

Slope 1m FPA			Slope 1m LPG		Slope 2m LPG	
Number of values	3355744	Number of values	Number of values	3355744	Number of values	839504
Minimum	0	Minimum	Minimum	0	Minimum	0
Maximum	84.58	Maximum	Maximum	67.22	Maximum	51.26
Range	84.58	Range	Range	67.22	Range	51.26
Mean	5.5135	Mean	Mean	2.583	Mean	1.792
Standard deviation	13.059	Standard deviation	Standard deviation	3.376	Standard deviation	2.9405
Skew	3.694	Skew	Skew	5.444	Skew	5.96

Slope 5m LPG		Slope 10m LPG	
Number of values	134680	Number of values	33744
Minimum	0	Minimum	0
Maximum	32.91	Maximum	21.42
Range	32.91	Range	21.42
Mean	1.2137	Mean	0.88408
Standard deviation	2.1507	Standard deviation	1.4057
Skew	6.229	Skew	5.929

Tab 4.2: Statistics for the various LiDAR DSM and derived slope values.

4.7 LiDAR Laser Intensity

LiDAR intensity data provides an indication of the intensity or amplitude of the reflection of the laser pulse from the ground surface. Many factors can affect the reflected laser intensity. Initial casual examination of LiDAR intensity data for the study areas suggests that there is a reduction in the intensity of the reflected light that corresponds with landscape features such as palaeochannels (Figs. 4.14, 4.15 and 4.31). Variations in the reflectivity of various earth surface materials to laser light of differing wavelength are quite well documented (for example see Wehr and Lohr, 1999: 74) and damp soil conditions are known to reduce reflectivity. It is possible that the increased soil moisture associated with palaeochannels and perhaps other associated variations in soil and vegetation properties, are responsible for the reduced reflectivity of the laser pulse. The present study has aimed to examine several aspects of LiDAR intensity data through visual comparison of intensity values with other ground and airborne remotely sensed data and though field measurement of volumetric soil moisture at selected sample locations.

4.8 Laser Intensity and Cropmark Formation

The analysis of LiDAR intensity data was undertaken largely within ArcGIS and ArcScene. Visual comparison of extracts from the intensity data with aerial photographic evidence and cropmark plots focused on examination of whether any aspects of the cultural archaeology, visible as crop or soilmarks on conventional aerial photographs, were evident in the intensity data. An extract from the June 1976 vertical photograph of the study area (Fairey Surveys 1861 7615) with excellent cropmark formation was geocorrected to accurately fit the LiDAR intensity image using ArcGIS. Published plots for the cropmarks for the Lockington villa and later prehistoric settlement complex (Ripper & Butler 1999) were scanned and similarly georeferenced to the LiDAR intensity data.

These data were visually compared within ArcGIS, using the GIS to produce accurately co-registered images showing in each instance; the air-photograph, colour-shaded intensity data, air-photograph and intensity data merged and the cropmark plot. In addition, the air-photographic and intensity data were similarly compared with the results of geophysical survey of the Warren Lane complex (Ripper & Butler 1999) and previously unplotted cropmarks on the Hemington terrace. LiDAR intensity readings were extracted for the elevation profiles examined in section 3.3. Visual examination of these intensity profiles (Figs. 4.18 – 4.23) assisted in understanding how intensity values vary in relation to elevation and topographical features.

4.8.1 LiDAR Intensity and Cropmark Formation

In general there appears to be a good degree of correlation between areas of higher LiDAR intensity and areas of cropmark formation, although no convincing cases of anthropogenic features evident as cropmarks could be seen in the LiDAR data. Figure 4.32 shows the Lockington villa and prehistoric settlement complex, located on the Holme Pierrepont sand and gravel (terrace 2) at the southern edge of the study area. As well as well defined cropmarks, the air photograph shows clear variations in the character of the soil and subsoil, represented by broad darker banks probably indicating deeper and/or clayey/silty subsoil. Cropmark formation is poor or non-existent on these darker bands and is largely confined to the areas of paler subsoil.

LiDAR intensity data reflects these broad subsoil divisions. The darker/silty subsoil correlates with darker bands on the air photograph, seen as areas of low LiDAR intensity and paler areas as high intensity. Merging the intensity and air-photographic images clearly shows that the low LiDAR intensity, coloured blue on Figure 4.32, coincides with the dark subsoil bands seen on the air-photograph.

Closer examination of the cropmark and intensity data (Figs 4.33 and 4.34) show that although there is a detailed correlation between subsoil effects on crop growth (seen on the air photos) and LiDAR intensity value, no actual cropmark features are evident in the intensity data. However, crop tramlines and the presence of a footpath (seen in Fig. 4.33 as a low intensity band crossing the villa site from north-west to south-east) indicate that the spatial resolution of the intensity data should be sufficiently fine to capture cropmark features. It is possible that at the time of the LiDAR survey flight ground conditions were not favourable to cropmark formation (which requires dry soil conditions inducing moisture stress in crops and allowing contrasts in available soil moisture and nutrients over buried archaeological features to affect crop growth). Similar factors area likely to affect LiDAR intensity readings, since soil moisture is thought to be the main contributor to variations in reflected laser intensity. Put simply, if conditions were not favourable to the formation of cropmarks (the survey flight was made during February 2003 which was relatively dry, with only 20.2mm rain reported by the nearest weather station at Sutton Bonington, as opposed to a monthly average on 50mm – data from Met Office) they may also have not favoured detection of anthropogenic features using LiDAR.

Figure 4.35 shows a further comparison of cropmark and intensity data, in this instance the cropmarks are those of a small sub-square D shaped enclosure, partly obscured by palaeochannels formation, within the Hemington terrace deposits at SK484300. The cropmark and channels are clearly defined on the air-photography. LiDAR intensity data shows some slight variations in intensity value that hints at the pattern of palaeochannels evident on the air-photograph, but is otherwise unhelpful.

Together, this evidence suggest that LiDAR intensity data is of limited use in detecting buried anthropogenic features as it does not function outside of the parameters (dry conditions, crops experiencing moisture stress) in which such features may anyway be detected by cropmarks. It would nonetheless be useful to examine LiDAR intensity data acquired at a time of good cropmark formation to investigate the possibility that intensity readings may reveal features or levels of detail not visible as cropmarks alone.

Finally, Figure 4.36 shows a comparison of air-photography, LiDAR intensity and geophysical (magnetometer) survey results for the Warren Lane later prehistoric settlement complex located on the Holme Pierrepont Sand and Gravel. Variations in LiDAR intensity in this image to some extent reflect subsoil character as revealed by the air-photograph, but appear largely to be a product of the different crops present in the two fields imaged. Both LiDAR and air-photography fail to reveal the wealth of sub-surface anthropogenic features identified by the magnetometer survey. These cautionary results highlight the need to pursue complimentary remote sensing campaigns in environments as complex and geomorphologically heterogeneous as a river confluence zone.

4.9 LiDAR Intensity and Topography

Figures 4.18 – 4.23 provide LiDAR intensity profiles for the 12 elevation profiles examined as part of the investigation of LiDAR DSM resolution. It can be seen that intensity levels vary closely in relation to elevation such that low elevation features correspond to areas of low intensity ands vice versa. In general variations in LiDAR intensity are likely to reflect soil and subsoil characteristic of the lower elevation areas, rather than be a direct reflection of elevation. The majority of the lower elevation features indicate

geomorphological features such as ridge and swale (Fig. 4.18) and palaeochannels (Figs. 4.19, 4.22 – 4.23). Areas of palaeochannels provide a particularly strong coincidence of variation in intensity and elevation and in some cases intensity variation exaggerate the effects of relatively slight variations in elevation (for example Figs. 4.21 and 4.22). It seems likely that intensity levels are largely affected by the increase in soil moisture prevalent in palaeochannels compared to the surrounding landscape.

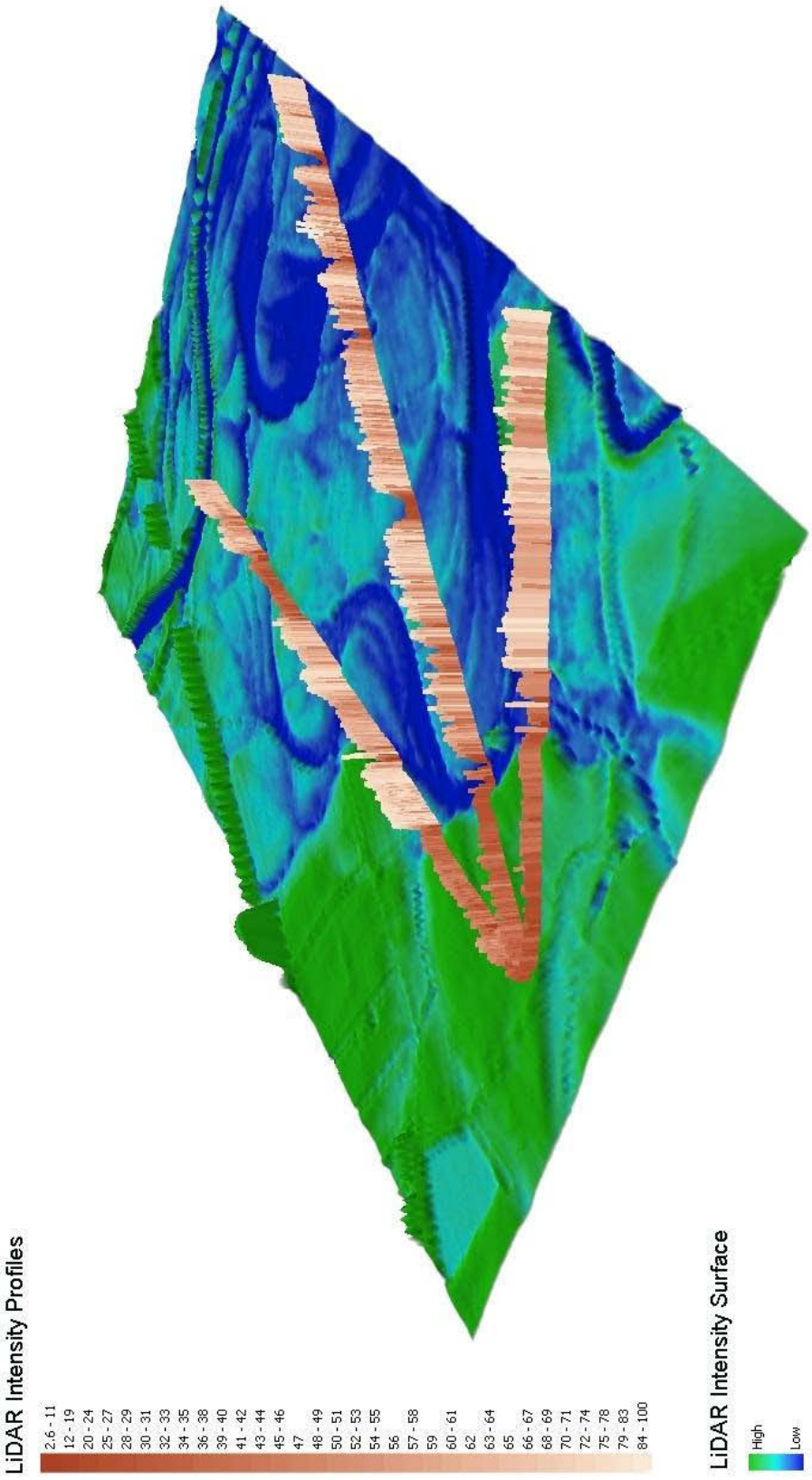

Fig 4.31: Pseudo 3D view of the LiDAR LP DSM of the study area colour shaded to reflect variations in laser intensity. The extruded profiles show variations in intensity data along each profile line as variations in height of the profile and colour shading of the profile bar.

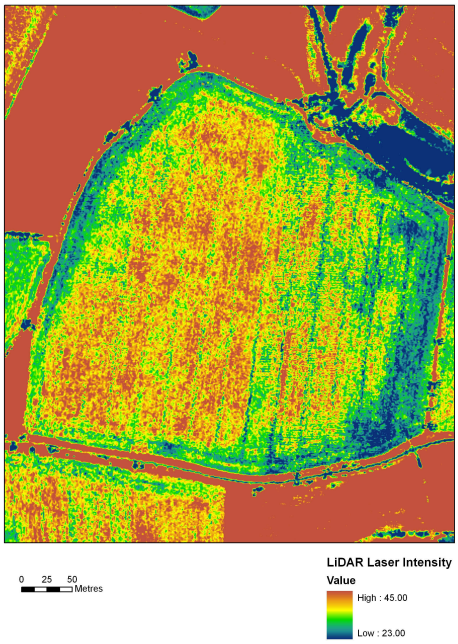

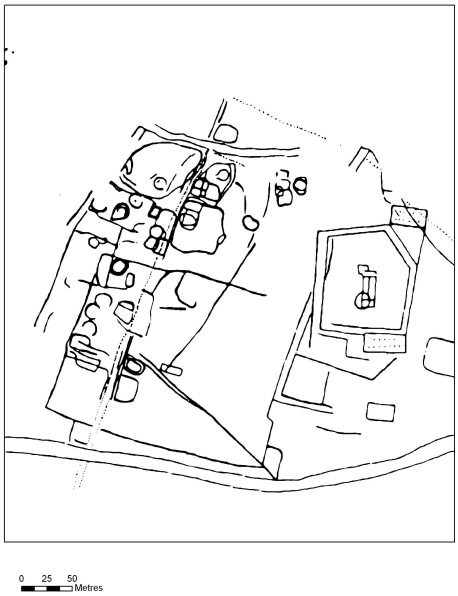

Fig 4.32: Comparison of (A) cropmark evidence on air photography, (B) LiDAR intensity, (C) intensity and cropmark evidence merged and (D) cropmark plot, for the later prehistoric settlement complex and Romano-British villa at Lockington.

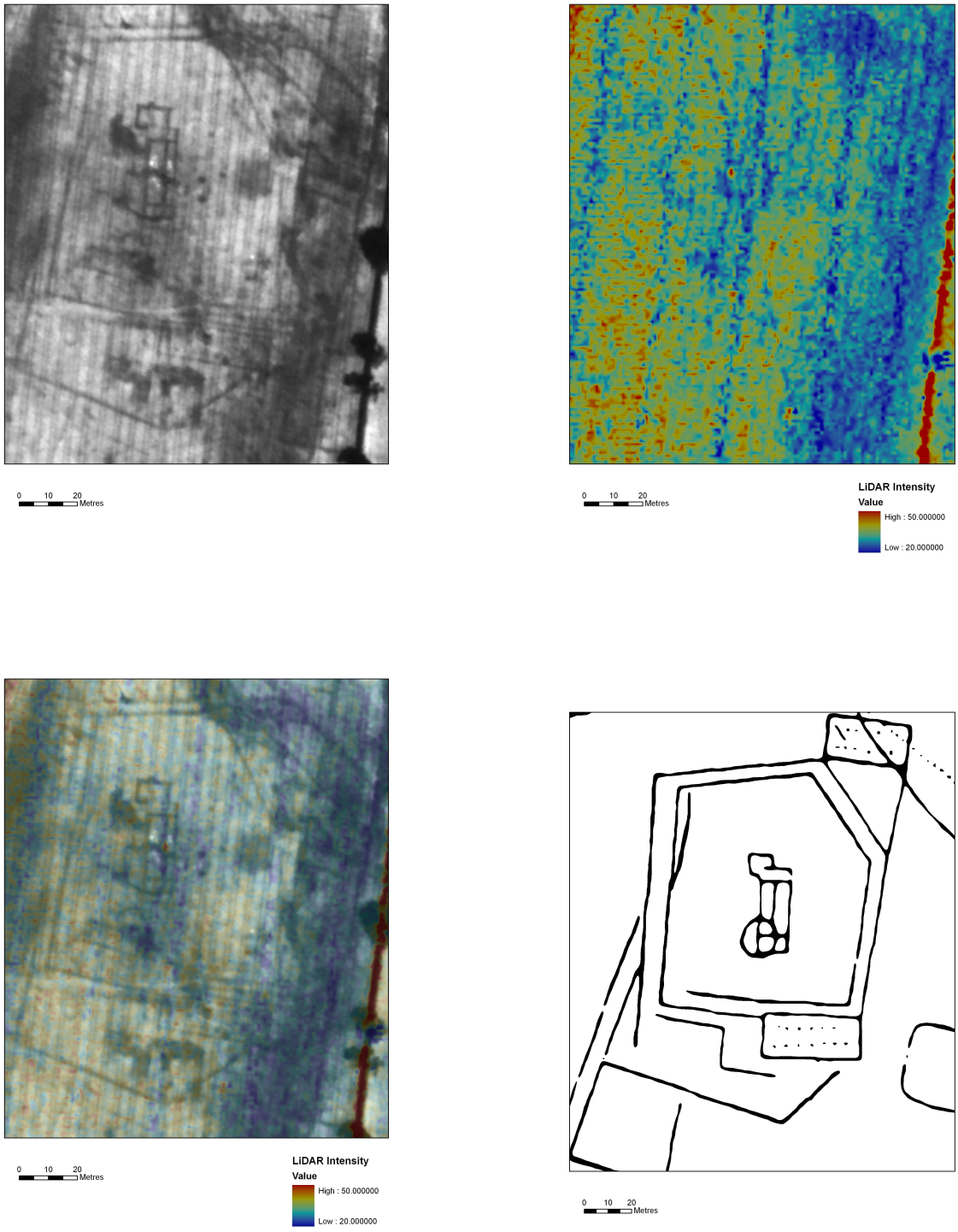

Fig 4.33: Comparison of (A) cropmark evidence on air photography, (B) LiDAR intensity, (C) intensity and cropmark evident merged and (D) cropmark plot, for the Lockington villa.

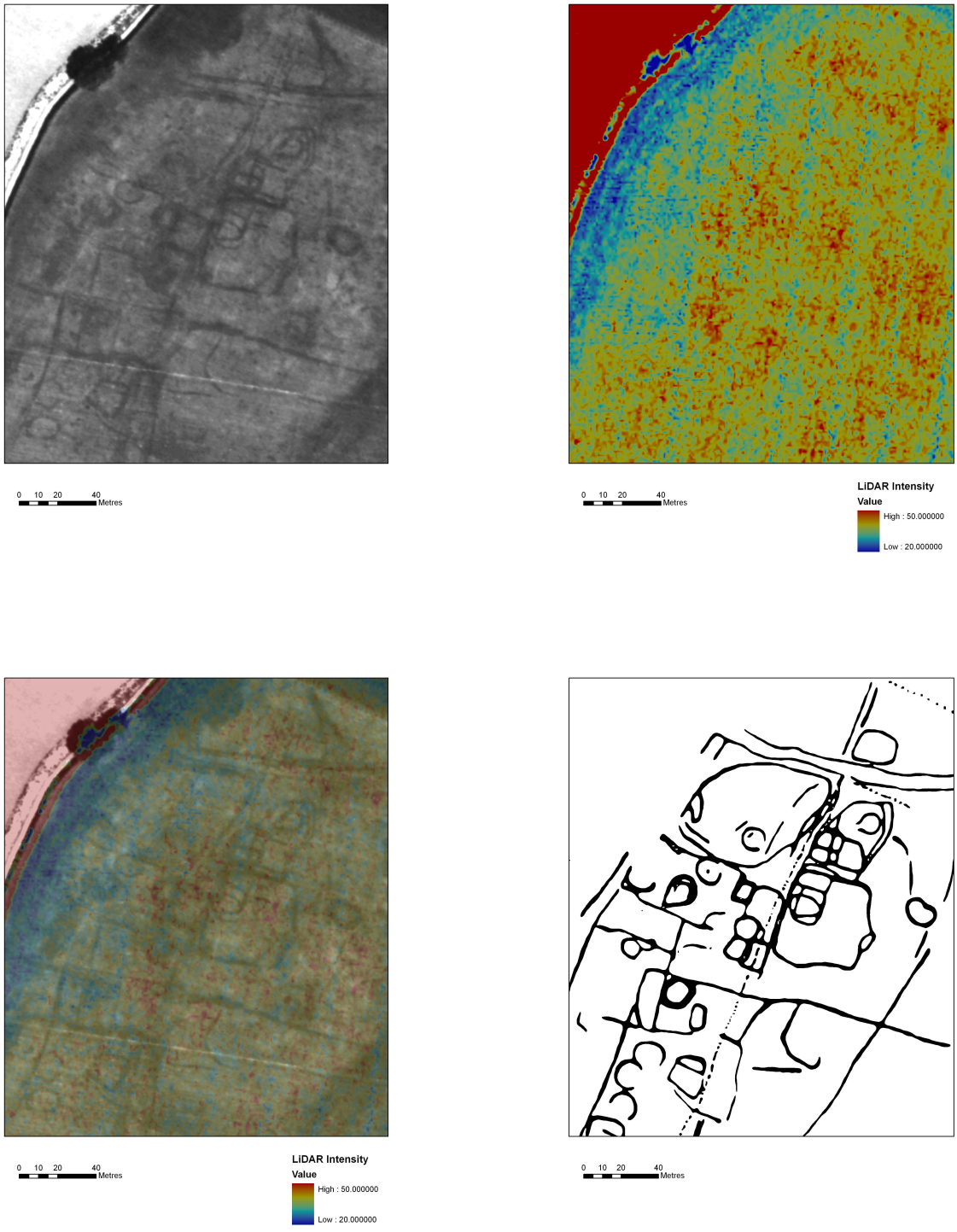

Fig 4.34: Comparison of (A) cropmark evidence on air photography, (B) LiDAR intensity, (C) intensity and cropmark evident merged and (D) cropmark plot, for the later prehistoric settlement complex at Lockington.

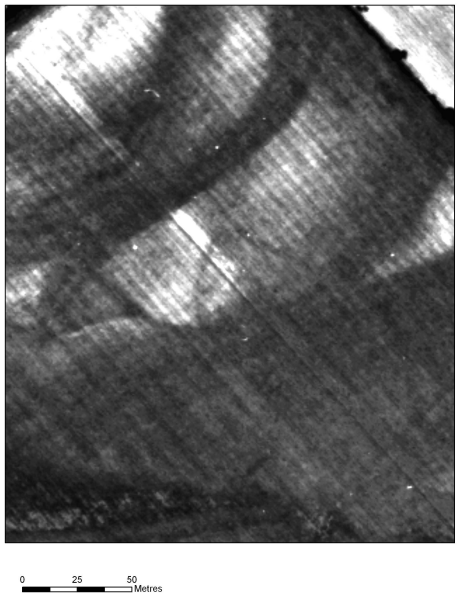

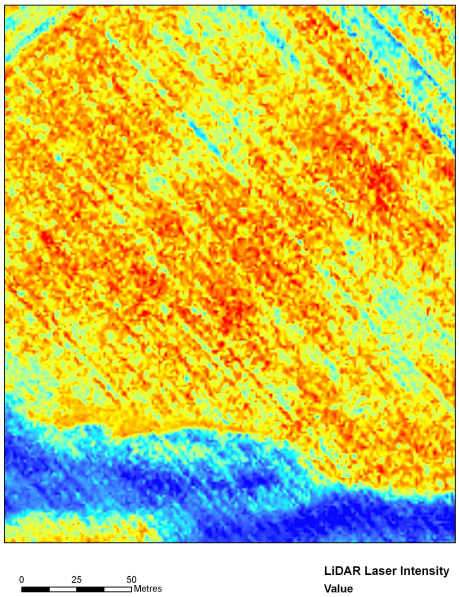

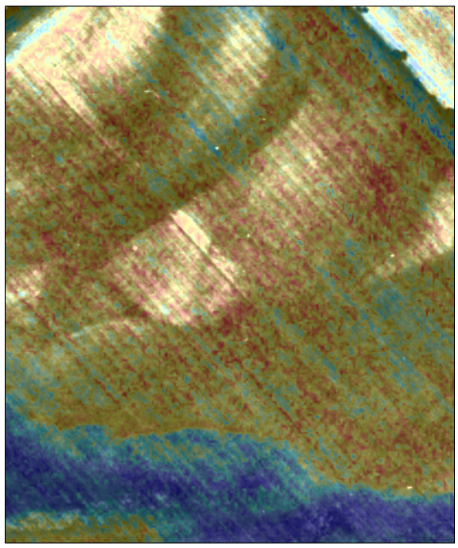

Fig 4.35: Comparison of (A) cropmark evidence on air photography, (B) LiDAR intensity, (C) intensity and cropmark evident merged and (D) cropmark plot, for the small sub-square D shaped enclosure at SK484300

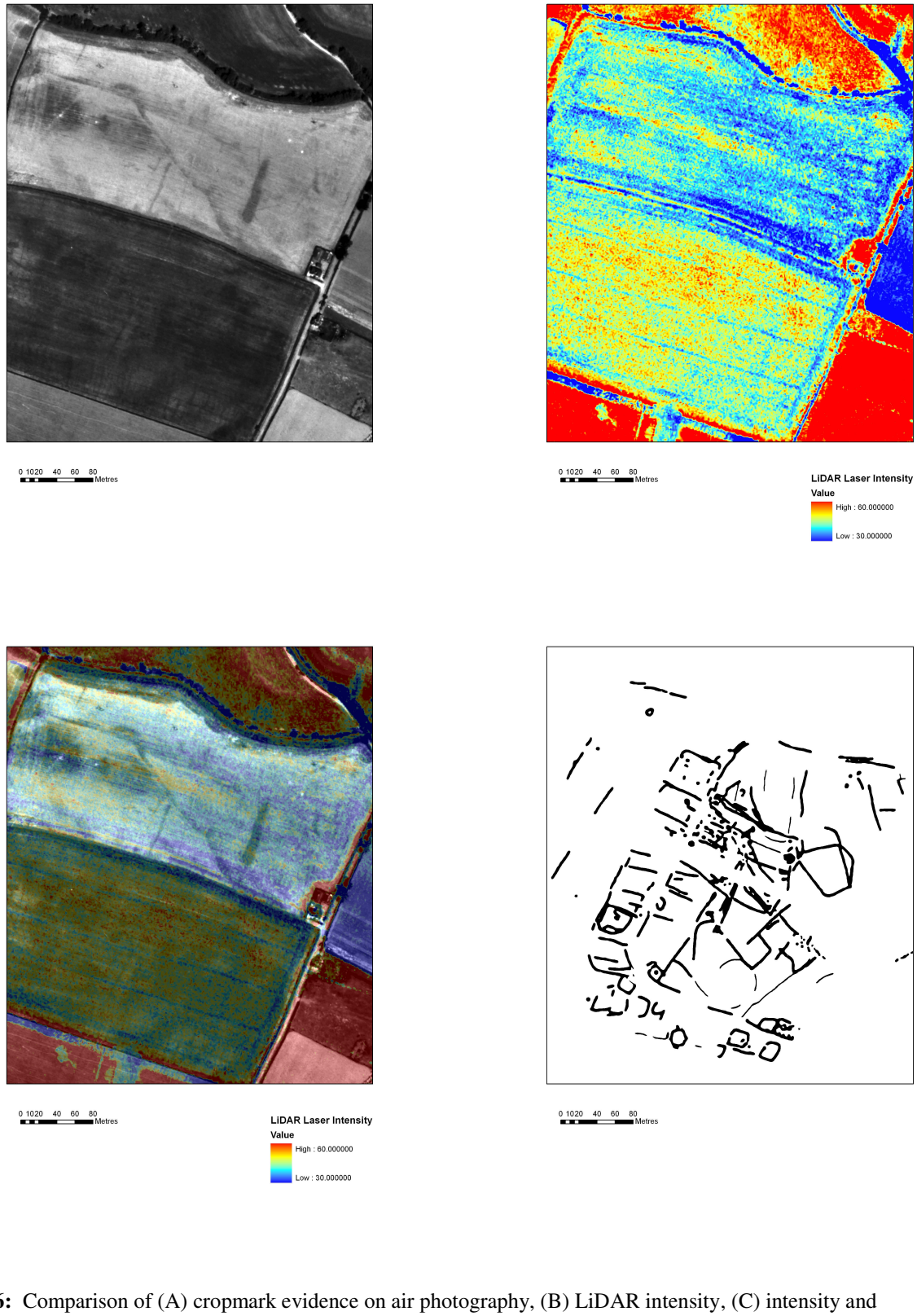

Fig 4.36: Comparison of (A) cropmark evidence on air photography, (B) LiDAR intensity, (C) intensity and cropmark evident merged and (D) geophysical survey plot, for the later prehistoric settlement complex at Warren Lane.